

Coherent Phonon Pairs and Rotational Symmetry Breaking of Charge Density Wave Order in the Kagome Metal CsV_3Sb_5

Qinwen Deng,¹ Hengxin Tan,² Brenden R. Ortiz,^{3,4} Andrea Capa Salinas,³ Stephen D. Wilson,³ Binghai Yan,² and Liang Wu^{1,*}

¹*Department of Physics and Astronomy, University of Pennsylvania, Philadelphia, Pennsylvania 19104, U.S.A*

²*Department of Condensed Matter Physics, Weizmann Institute of Science, Rehovot, Israel*

³*Materials Department, University of California Santa Barbara, Santa Barbara, California 93106, U.S.A.*

⁴*Materials Science and Technology Division, Oak Ridge National Laboratory, Oak Ridge, Tennessee 37831, United States*

(Dated: March 11, 2025)

In this work, we perform ultrafast time-resolved reflectivity measurements to study the symmetry breaking in the charge-density wave (CDW) phase of CsV_3Sb_5 . By extracting the coherent phonon spectrum in the CDW phase of CsV_3Sb_5 , we discover close phonon pairs near 1.3 THz and 3.1 THz, as well as a new mode at 1.84 THz. The 1.3 THz phonon pair and the 1.84 THz mode are observed up to the CDW transition temperature. Combining density-functional theory calculations, we point out these phonon pairs arise from the coexistence of Star-of-David and inverse Star-of-David distortions combined with six-fold rotational symmetry breaking. An anisotropy in the magnitude of transient reflectivity change is also revealed at the onset of CDW order. Our results thus indicate broken six-fold rotational symmetry in the charge-density wave state of CsV_3Sb_5 , along with the absence of nematic fluctuation above T_{CDW} . Meanwhile, the measured coherent phonon spectrum in the CDW phase of $\text{CsV}_3\text{Sb}_{5-x}\text{Sn}_x$ with $x = 0.03-0.04$ matches with staggered inverse Star-of-David with interlayer π phase shift. This CDW structure contrasts with undoped CsV_3Sb_5 and explains the evolution from phonon pair to a single mode at 1.3 THz by $x = 0.03-0.04$ Sn-doping.

The Kagome lattice, hosting a corner-sharing triangle network, has been the focus of extensive research for decades due to its interplay of inherent geometrical frustrations, nontrivial topology and unconventional correlation effects. As a recent example, the newly discovered vanadium-based Kagome superconductors AV_3Sb_5 ($A = \text{K}, \text{Rb}$ or Cs) have attracted tremendous research interest due to their unconventional electronic landscape, including charge density wave (CDW) below $T_{\text{CDW}} \approx 78-102$ K and superconductivity with $T_c \approx 0.9-2.5$ K[1–4]. More intriguingly, additional exotic electronic instabilities emerge inside the CDW phase, including signatures of a possible time-reversal symmetry breaking loop current state[5–16], electronic nematicity[17–22], and pair density wave within the superconducting state[23]. Therefore, it is of paramount significance to clarify the structure and symmetry of the CDW order in this family of compounds, in order to understand the interaction between this plethora of charge orders and superconductivity.

An abundance of initial experiments reported a 3D CDW state in AV_3Sb_5 [24–26]. Among all members in this family of materials, CsV_3Sb_5 possesses the largest variety of reported 3D CDW phases with different interlayer stacking orders. These 3D CDW orders can be constructed from unstable phonon modes at M and L points in the momentum space which give rise to various $2 \times 2 \times 2$ CDW patterns[27–29]. The in-plane 2×2 distortions on the Kagome lattice can be characterized by either a Star-of-David (SD) or inverse Star-of-David (ISD) pat-

tern [10, 27, 29] (Fig. 1a, b), with a well-defined phasing of 0 or π between neighboring Kagome layers. The relative energy of different CDW structures is very close, and consensus has not been made on the precise ground state configuration despite extensive research. Different measurements mainly evidenced either the LLL phase with alternative SD + ISD without interlayer π phase shift [30–34] (Fig. 1d), in which the six-fold rotational symmetry C_6 is preserved, or the MLL phase with ISD + ISD with interlayer π phase shift[9, 35–39] (Fig. 1c), in which the six-fold rotational symmetry is broken down to two-fold. A further $2 \times 2 \times 4$ supercell was also reported to coexist and compete with the $2 \times 2 \times 2$ structures [37, 40] as observed by X-ray diffraction, with contradicting results whether this $2 \times 2 \times 4$ phase only has C_2 [26, 37, 40, 41]. This is possibly due to the phase coexistence, locally of multiple CDW ordered states as reported by recent dark-field X-ray results[42]. Apart from whether the system breaks six-fold rotational symmetry, another major debate is at what temperature the six-fold symmetry breaks. Various experimental probes produced conflicting results regarding the onset temperature of rotational symmetry breaking, either at T_{CDW} [9, 40, 43] or much lower than T_{CDW} [8, 17–19, 44] via a distinct electronic nematic state. Therefore, whether the two-fold symmetry is directly related to the CDW has not yet been made clear. Another important question is whether fluctuations of these exotic electronic states emerge above T_{CDW} in CsV_3Sb_5 . Strong CDW fluctuations and nematic states have been reported above T_{CDW} [21, 45, 46], although recent strain dependent measurements showed no fluctuating vestigial nematicity[22].

In this work, we use ultrafast time-resolved reflectivity (TR-reflectivity) experiments to study the struc-

*Electronic address: liangwu@sas.upenn.edu

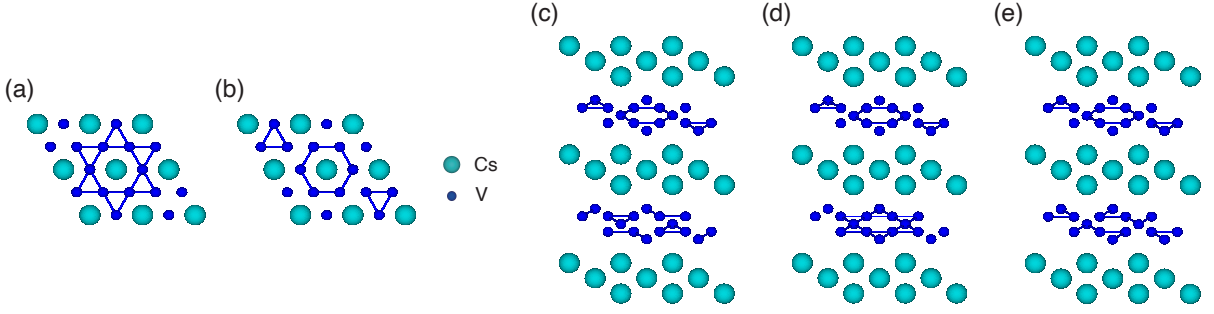


FIG. 1: **CDW distortions in CsV_3Sb_5 .** (a) $2 \times 2 \times 1$ SD. (b) $2 \times 2 \times 1$ ISD. (c) ISD + ISD with interlayer π -phase shift, (d) SD + ISD without interlayer phase shift, and (e) SD + ISD with interlayer π -phase shift. The Cs atoms are shown in cyan and V atoms are shown in blue. The Sb atoms are not shown for simplicity. Note that only the structure in (a, b, d) keeps the D_{6h} symmetry. The lines connecting V atoms indicate shorter V-V bonds.

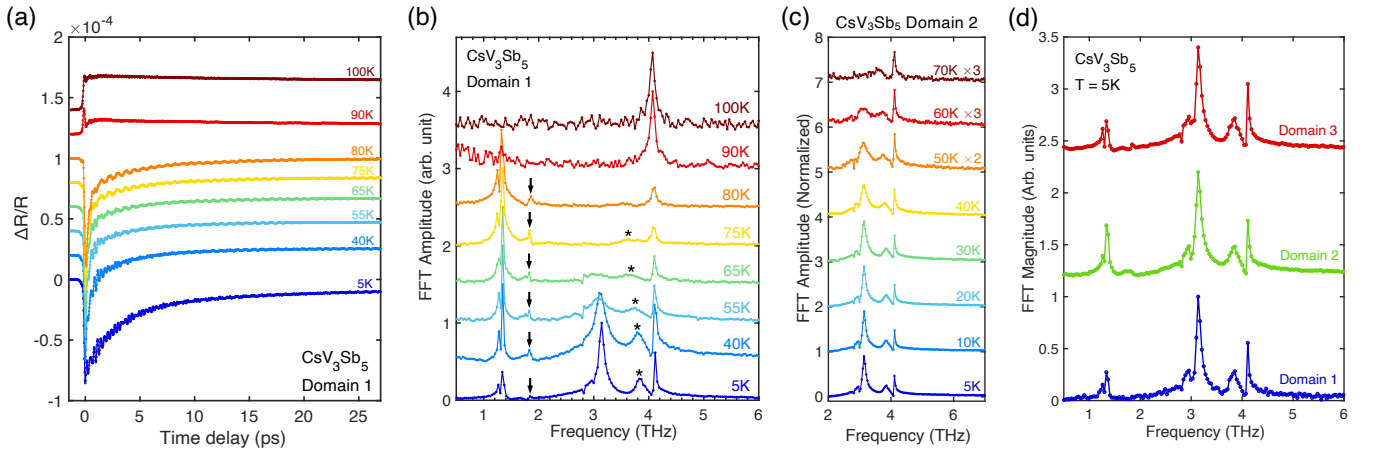


FIG. 2: **Temperature-dependent coherent phonon spectroscopy in Kagome CsV_3Sb_5 .** (a) Time-resolved reflectivity curves at different temperatures above and below T_{CDW} in a single birefringence domain. (b) Amplitudes of Fourier transforms of coherent phonon oscillations in (a) after subtracting a double-exponential background. The arrow marks the temperature evolution of the 1.84 THz mode, and the asterisk marks the temperature evolution of the 3.86 THz mode. (c) Same as (b) but measured in another birefringence domain and zoomed in around 4 THz to better show the two close modes near 3.1 THz. All datasets are normalized to its maximum amplitude. (d) Coherent phonon spectrum measured on all 3 different birefringence domains at 5 K. Curves are offset for clarity in all plots.

tural symmetry of the CDW phase of CsV_3Sb_5 . The derived coherent phonon spectrum reveals close phonon pairs at 1.3 and 3.1 THz and a newly discovered mode at 1.84 THz. The 1.3 THz phonon pair and the 1.84 THz mode persist up to T_{CDW} . By comparing the calculated phonon frequencies using density functional theory (DFT), we demonstrate the close phonon pairs can only be explained via the coexistence of SD and ISD pattern combined with six-fold rotational symmetry breaking. An anisotropy of the transient reflectivity change ($\Delta R/R$), defined as non-equal $\Delta R/R$ values between two orthogonal polarization directions, also occurs upon entering CDW state. Our results thus unequivocally corroborate six-fold rotational symmetry breaking in the CDW phase of CsV_3Sb_5 . Meanwhile, we pinpoint the CDW structure of $\text{CsV}_3\text{Sb}_{5-x}\text{Sn}_x$ with $x = 0.03-0.04$ to

ISD + ISD with interlayer π -phase shift, which reduces the 1.3 THz phonon pair to a single phonon mode.

CsV_3Sb_5 single crystals are synthesized using the self-flux method[1, 3]. We perform TR-reflectivity measurements on freshly cleaved (001) surface of CsV_3Sb_5 single crystals. For all pump-probe experiments, pump wavelength is at 1560 nm and probe wavelength is at 780 nm, with repetition rate of 80 MHz and pulse duration of 100 fs. To reduce sample heating, both beams have a fluence less than $10 \mu\text{J}/\text{cm}^2$. Both beams are focused by an objective lens to achieve a spot size of $\sim 10 \mu\text{m}$ in diameter. In our previous experiments[9], we pinpointed the three-state birefringence domains in CsV_3Sb_5 below T_{CDW} , with the domain size being $\sim 100 \mu\text{m}$. We can thus probe the transient reflectivity change in a single birefringence domain. Here, we use an xyz-stage to carefully adjust the

light spot position onto a selected birefringence domain. The pump beam intensity is modulated at a frequency of 84 kHz using a photo-elastic modulator.

The coherent phonon generation via the pump pulse modulates the refractive index by the ion motion[47–49] which causes transient reflectivity changes. Fig. 2a shows the transient reflectivity change ($\Delta R/R$) versus the pump-probe time delay measured inside a single birefringence domain of CsV_3Sb_5 at different temperatures. A single phonon oscillation can be observed above the CDW transition temperature $T_{\text{CDW}} \sim 90$ K. In contrast, the sign of the transient reflectivity traces flips below T_{CDW} , with the emergence of multiple phonon modes, as can be observed from the complex oscillation pattern. To better understand the evolution of coherent phonon modes as a function of temperature in the CDW phase, a double exponential decay background ($A_0 + A_1 \exp(-t/\tau_1) + A_2 \exp(-t/\tau_2)$) is fitted to all time traces and then subtracted to show the oscillation parts, which are then Fourier transformed to reveal the coherent phonon modes (Fig. 2b). Above T_{CDW} , only one mode at 4.1 THz exists. This 4.1 THz mode persists at all temperatures and should be assigned as a main lattice mode. Indeed, it matches with a 4.10 THz A_{1g} mode in the pristine phase of CsV_3Sb_5 (Table I). In contrast, at $T = 5$ K, another two intense modes centered at 1.3 and 3.1 THz are conspicuously present, similar to previous pump-probe reflectivity studies[36, 50]. As temperature increases, the 1.3 THz mode exhibits an increase in amplitude but an abrupt disappearance at $T \approx 90$ K, matching with reported $T_{\text{CDW}} = 94$ K[2, 51]. We note modest local laser heating may cause a slight decrease of the measured T_{CDW} . Little frequency softening is seen for the 1.3 THz mode when increasing the temperature, more consistent with a zone-folded phonon mode by CDW[52]. This explains its disappearance in the phonon spectrum above T_{CDW} . In contrast, the amplitude of 3.1 THz mode decreases during warm-up and vanishes at ~ 65 K (Fig. 2b, c). Previous Raman studies [53, 54] showed this 3.1 THz mode exhibits significant weakening and broadening upon warming toward T_{CDW} , becoming overdamped between 60 and 90 K with the linewidth as large as 50 cm^{-1} right below T_{CDW} . This may explain why this 3.1 THz mode vanishes in our detection above ~ 65 K. Apart from these dominant modes, we also find a 3.86 THz mode and a weaker 1.84 THz mode that is newly-discovered by time-resolved reflectivity (Fig. 2b). Similar to the 1.3 THz mode, the 1.84 THz mode also shows little frequency change and persists up to T_{CDW} . We do not observe other modes up to 15 THz.

Contrary to previously reported pump-probe experiments on CsV_3Sb_5 [36, 43, 50], we observe clear close phonon pairs near both 1.3 THz and 3.1 THz in our phonon spectrum. At $T = 5$ K, the 1.3 THz mode consists of two close phonon modes as shown in Fig. 2b with two peaks centered at 1.26 THz and 1.33 THz, respectively. These dual modes persists upon warming, up to T_{CDW} where it vanishes. Additionally, two close phonon

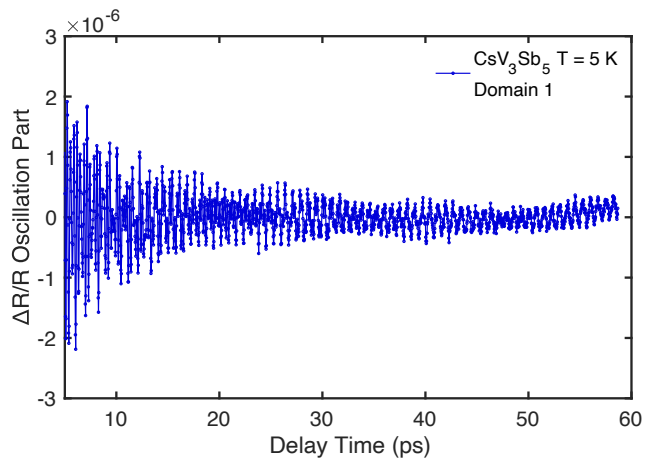


FIG. 3: Oscillation part of the TR-reflectivity curve corresponding to the phonon spectrum of domain 1 in Fig. 2. Clear beatings can be observed in the oscillation pattern which corroborates the dual modes near 1.3 THz. The data is taken at $T = 5$ K.

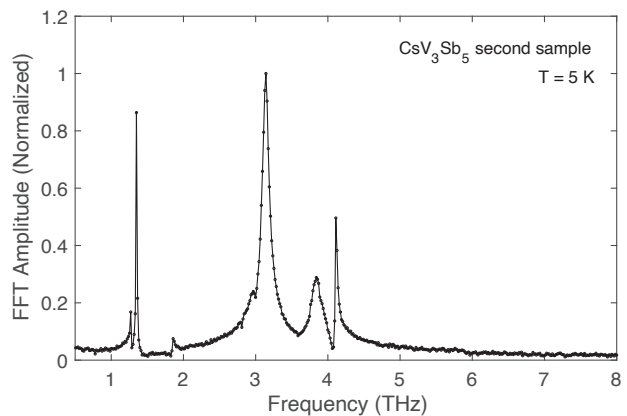


FIG. 4: Coherent phonon spectrum measured by TR-reflectivity on a second CsV_3Sb_5 sample at $T = 5$ K. It also shows the dual modes at 1.3 THz and 3.1 THz, as well as the newly discovered weaker mode near 1.8 THz.

peaks correspond to beatings in the time domain. Indeed, the beating waveform arising from these dual modes near 1.3 THz can be resolved in longer time scans (Fig. 3) with delay time difference of ~ 14 ps between wave nodes, in accordance with the frequency splitting (~ 0.07 THz) between these two peaks. Repeated measurements on another CsV_3Sb_5 sample also shows this 1.3 THz dual modes (Fig. 4). Meanwhile, same experiments on a second birefringence domain (Fig. 2c and Domain 2 in Fig. 2d) visualizes two close phonon modes near 3.1 THz, with its two peaks centered at 2.96 THz and 3.14 THz at $T = 5$ K. These two close modes persist up to 60 K when the 3.1 THz mode fades away in our detection. Moreover, both 1.3 and 3.1 THz phonon pairs are visible in the coherent phonon spectrum extracted from all three

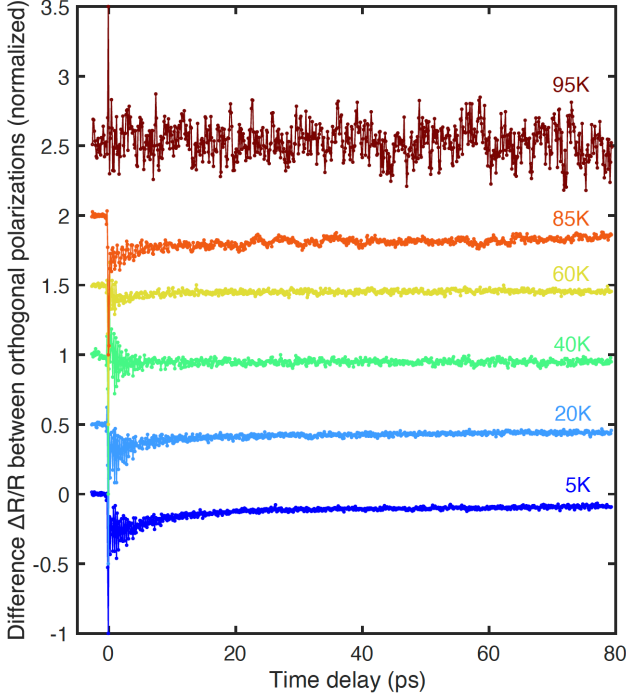


FIG. 5: Differential time-resolved reflectivity curves between orthogonal incident probe polarizations at different temperatures across T_{CDW} . All curves are normalized by their peak values at $t = 0$ ps and offset for clarity. The light spot position is inside a single birefringence domain. Nonzero differential values below T_{CDW} indicates in-plane anisotropy, suggesting C_6 is broken. However, no difference is observed beyond noise level above T_{CDW} , indicating the preserve of C_6 and absence of nematic fluctuations.

birefringence domains (Fig. 2d).

Furthermore, we reveal evidence of C_6 breaking from the anisotropy of transient reflectivity response by varying probe polarizations, which manifests breaking of rotational symmetry and has been used to study the nematic order in Fe-based superconductors[55–57]. By varying the probe polarization within the (001) surface, we observe the anisotropic transient reflectivity signal inside the Kagome plane at $T = 5$ K, indicating broken C_6 . To highlight this anisotropy, we subtract the signals from orthogonal probe polarization states that correspond to maximum and minimum signal size respectively. As shown in Fig. 5, this anisotropy persists in the CDW phase but vanishes above T_{CDW} , corroborating C_6 breaking onsets at the CDW transition. This is different from the low-temperature electronic nematic order seen by NMR[17] and STM quasiparticle interference measurement[18, 44] that onsets at ~ 35 K far below T_{CDW} . Our observed isotropic response of transient reflectivity above T_{CDW} demonstrates C_6 symmetry, sharing the conclusion of Liu et al.[22] suggesting no vestigial nematic order associated with the C_6 -breaking CDW.

To explain the observed close phonon modes and deter-

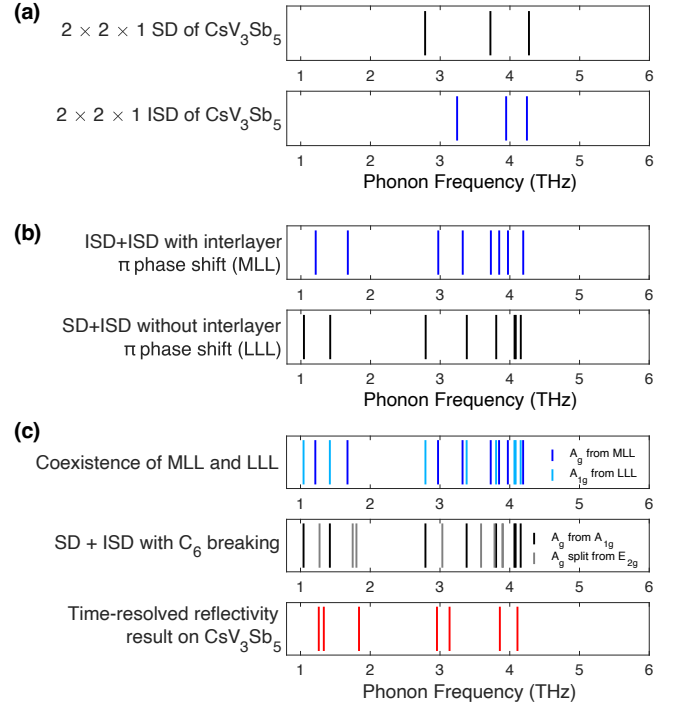


FIG. 6: **Comparison of the DFT results and the measured phonon modes by TR-reflectivity on CsV_3Sb_5 at $T = 5$ K.** The vertical lines denote the frequency of the $A_{1g}(A_g)$ modes in DFT calculation results or the measured phonon frequency. For DFT-calculated phonons, only the modes below 4.5 THz are shown. (a) The calculated A_{1g} mode frequencies in SD and ISD CDW phases in CsV_3Sb_5 . (b) The calculated A_g (A_{1g}) mode frequencies in the ISD + ISD with interlayer π phase shift (SD + ISD without interlayer π phase shift) CDW order. (c) The calculated fully-symmetric mode frequencies in the CDW order with the coexistence of MLL and LLL, and the calculated A_g mode frequencies in SD + ISD with C_6 breaking CDW phases in CsV_3Sb_5 and their comparison to the observed phonon modes in our TR-reflectivity results.

mine the CDW structure of CsV_3Sb_5 , we perform DFT calculations of phonon frequencies and compare with the phonon spectrum detected by TR-reflectivity. In TR-reflectivity measurements, the femtosecond pump pulse selectively excites Raman-active phonons coherently[58, 59]. On the theory side, coherent phonon excitation is often described either as impulsive stimulated Raman scattering (ISRS)[60–62] or as displacive excitation of coherent phonons (DECP)[63, 64]. In ISRS, there is no restrictions on the symmetry of the Raman-active modes[60], and ISRS does not require absorption in the material[65, 66]. Meanwhile, DECP requires absorption at the pump frequency in order to disturb the electronic energy distribution in the material, and only fully symmetric modes can be observed[63, 64] in DECP mechanism. Fully symmetric phonon modes host Γ_1^+ symmetry, such as A_{1g} modes in D_{6h} point group and A_g modes in D_{2h} point group.

Pristine	A_{1g}	E_{2g}							
	4.10	3.86							
$2 \times 2 \times 1$ SD	A_{1g}	A_{1g}	A_{1g}	E_{2g}	E_{2g}	E_{2g}	E_{2g}		
	2.78	3.72	4.27	1.49	1.65	3.58	3.88		
$2 \times 2 \times 1$ ISD	A_{1g}	A_{1g}	A_{1g}	E_{2g}	E_{2g}	E_{2g}	E_{2g}		
	3.24	3.95	4.24	1.73	2.97	3.74	3.87		
ISD + ISD with interlayer π phase shift	A_g	A_g	A_g	A_g	A_g	A_g	A_g	A_g	A_g
	1.21	1.67	2.97	3.32	3.73	3.85	3.97	4.19	
SD + ISD without interlayer π phase shift	A_{1g}	A_{1g}	A_{1g}	A_{1g}	A_{1g}	A_{1g}	A_{1g}	A_{1g}	A_{1g}
	1.04	1.42	2.79	3.38	3.80	4.07	4.08	4.16	
	E_{2g}	E_{2g}	E_{2g}	E_{2g}	E_{2g}	E_{2g}	E_{2g}	E_{2g}	E_{2g}
	0.31	1.27	1.75	1.80	3.03	3.59	3.78	3.89	3.90

TABLE I: Frequency (unit: THz) of the selected Raman-active modes in the pristine and CDW phases of CsV_3Sb_5 calculated by DFT. Only relevant A_{1g} , E_{2g} and A_g modes with frequencies below 4.5 THz are included. When interlayer π phase shift between the SD and ISD layer is included, the E_{2g} modes in the SD + ISD without interlayer π phase shift (LLL) phase will split to induce A_g modes that can be detected in TR-reflectivity.

To determine the coherent phonon excitation mechanism in our pump-probe measurement, we first compare our detected phonon modes with previous Raman spectroscopy results on CsV_3Sb_5 [53, 67]. Above T_{CDW} , Raman spectroscopy detected one A_{1g} mode at 4.1 THz and one E_{2g} mode at 3.6 THz with comparable amplitudes. This main 3.6 THz E_{2g} mode persists across T_{CDW} at all temperatures and has the maximum amplitude among all non-fully-symmetric Raman-active modes, with minimal frequency change of less than 1 cm^{-1} ($\rightarrow 0.030 \text{ THz}$) and increasing amplitude as temperature increases[53, 67]. However, in our TR-reflectivity measurements, we only detect the 4.1 THz A_{1g} mode above T_{CDW} . Below T_{CDW} , we do not observe this strongest 3.6 THz E_{2g} mode either. The closest detected mode is the 3.86 THz mode, but it quickly weakens and softens as temperature increases, in contrast to the 3.6 THz E_{2g} mode. Since we do not observe this dominant 3.6 THz mode at any temperature, we can rule out the detection of non-fully-symmetric modes in our TR-reflectivity measurements. Meanwhile, our pump photon energy ($\sim 0.79 \text{ eV}$) is much larger than the partial CDW gap opening in CsV_3Sb_5 [34, 68–70] indicating strong absorption at pump frequency. Thus, we use the DECP mechanism to interpret our data, and we assume all the detected phonon modes in our time-resolved reflectivity measurements are fully symmetric modes. This also matches with a previous pump-probe study on CsV_3Sb_5 [36].

We first examine the phonon spectra of the two C_6 -symmetric $2 \times 2 \times 1$ CDW orders, SD and ISD, to see if they match with our observed phonon spectrum. Fig. 6a shows the DFT calculated A_{1g} phonon spectrum of SD and ISD phases in the relevant frequency region. Both phases lack the observed 1.3 and 3.1 THz phonon pairs and the 1.84 THz mode from our TR-reflectivity measurements.

Thus, we need to consider a modulation along c axis of the CDW order, which is consistent with previous X-ray diffraction studies[25, 40]. We first examine the two most reported $2 \times 2 \times 2$ CDW states (Fig. 6b): either ISD + ISD with interlayer π phase shift (MLL), where the C_6 rotational symmetry is broken, or SD + ISD without interlayer π phase shift (LLL), where C_6 is preserved. The calculated fully-symmetric A_g (A_{1g}) mode frequencies in the ISD + ISD with interlayer π phase shift (SD + ISD without interlayer π phase shift) CDW order has been listed in Table I and plotted in Fig. 6b. The MLL phase agrees with our TR-reflectivity results better, with the frequency difference of the two A_g modes near 3.1 THz closer to the observed value. The MLL phase also hosts an A_g mode at 1.67 THz that matches the observed 1.84 THz phonon. This A_g mode comes from the C_6 -breaking induced split of an E_{2g} mode at 1.73 THz in $2 \times 2 \times 1$ ISD phase (Table I) ($E_{2g} \rightarrow A_g + B_{1g}$). However, MLL only shows one A_g mode near 1.3 THz, which fails to explain the observed two close modes near 1.3 THz. For the LLL phase, although it has two A_{1g} phonon pairs near 1.3 THz and 3.1 THz, their frequency differences are too large to match the measured values of our observed 1.3 THz and 3.1 THz phonon pairs. Also, no A_{1g} mode in LLL matches well with our observed 1.84 THz mode. Finally, our previous birefringence measurement indicates C_6 symmetry breaking[9], contradictory to the preserved C_6 in LLL.

However, if C_6 is broken by interlayer π phase shift between the SD and ISD layer (Fig. 1e), the E_{2g} modes in the C_6 -symmetric LLL phase will split to give rise to a fully symmetric A_g mode that can be detected in our TR-reflectivity measurements. The A_{1g} modes in the LLL phase will also evolve into A_g modes. We list the A_g modes in this C_6 -breaking SD + ISD state in Fig. 6c. In this C_6 -breaking SD + ISD state, there exists close 1.3

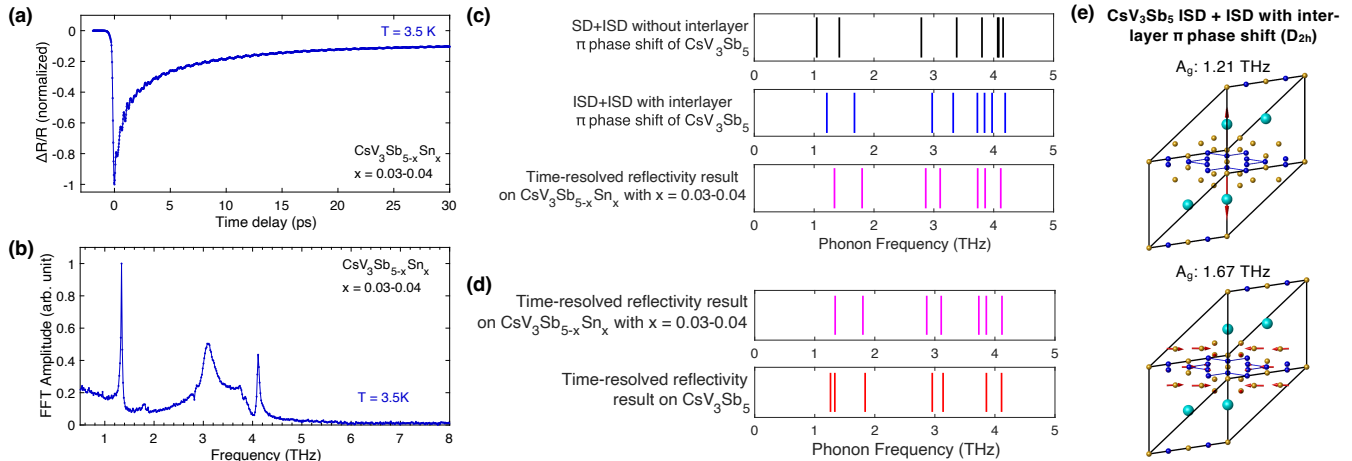


FIG. 7: **Coherent phonon spectrum in $\text{CsV}_3\text{Sb}_{5-x}\text{Sn}_x$ with $x = 0.03-0.04$.** (a) TR-reflectivity time trace on $\text{CsV}_3\text{Sb}_{5-x}\text{Sn}_x$ with $x = 0.03-0.04$ at $T = 3.5$ K. (b) Coherent phonon spectrum measured from TR-reflectivity at $T = 3.5$ K. (c) The calculated A_{1g} (A_g) mode frequencies in the SD + ISD without interlayer π phase shift (ISD + ISD with interlayer π phase shift) CDW state in CsV_3Sb_5 and their comparison to our TR-reflectivity results in $\text{CsV}_3\text{Sb}_{5-x}\text{Sn}_x$ with $x = 0.03-0.04$. (d) Comparison of the measured coherent phonon spectrum by time-resolved reflectivity in CsV_3Sb_5 and $\text{CsV}_3\text{Sb}_{5-x}\text{Sn}_x$ with $x = 0.03-0.04$. In (c-d), The phonon spectrum of $\text{CsV}_3\text{Sb}_{5-x}\text{Sn}_x$ with $x = 0.03-0.04$ measured from TR-reflectivity is taken at $T = 3.5$ K. In (d), the spectrum for CsV_3Sb_5 is taken at $T = 5$ K. (e) The DFT-calculated oscillation pattern of the fully-symmetric Raman active A_g modes in ISD + ISD with interlayer π phase shift (MLL) CDW state in CsV_3Sb_5 that are near our detected 1.34 and 1.80 THz modes in $\text{CsV}_3\text{Sb}_{5-x}\text{Sn}_x$ with $x = 0.03-0.04$ via time-resolved reflectivity, respectively. The 1.21 and 1.67 THz A_g modes are the lowest and second-lowest frequency mode in the A_g phonon spectrum of MLL phase in (c).

THz and 3.1 THz A_g pairs, along with A_g modes near 1.8 THz that are split from E_{2g} modes (e.g. the 1.75 and 1.80 THz E_{2g} mode in SD + ISD without interlayer π phase shift shown in Table I), matching our measured phonon spectrum better than merely MLL or LLL. While there are more A_g modes in calculation than observed, some modes could be missing in our observation, possibly due to their weaker modulations on the refractive index. Moreover, some calculated modes between 3.5 - 4 THz may be too close in frequency to be resolved individually in the measurements.

We also note a recent time-resolved X-ray diffraction measurement that demonstrated the coexistence of MLL and LLL CDW orders[71] which also breaks C_6 . By comparing the combined phonon spectrum of these two CDW orders, we point out this coexistence configuration can also explain our experimentally detected phonon spectrum (Fig. 6c) by showing fully-symmetric phonon pairs near 1.3 and 3.1 THz and a fully-symmetric mode near 1.8 THz. In either case, the two close phonon pairs near 1.3 and 3.1 THz observed in our TR-reflectivity measurement strongly corroborate C_6 -breaking in the CDW phase of CsV_3Sb_5 and the coexistence of SD and ISD patterns. Meanwhile, to explain our observed 1.84 THz mode, C_6 -breaking is also required in these $2 \times 2 \times 2$ CDW states to give rise to a fully symmetric A_g mode near 1.8 THz by splitting corresponding E_{2g} modes. Thus, the persistence of two close modes near 1.3 THz and the 1.84 THz mode up to T_{CDW} in our measurements marks the C_6 breaking happens simultaneously with the

onset of CDW, contrary to the electronic nematicity revealed by NMR[17] and STM[18, 44] that only onset at temperatures far below T_{CDW} .

There is also a recent Raman measurement reporting two close modes near 1.3 THz[39] but only above ~ 65 K. The temperature-dependent evolution of the intensities of these two modes indicated a spectral transformation between them and the higher frequency mode became weaker above ~ 65 K. This is different from our TR-reflectivity results where the two close modes near 1.3 THz are always present from T_{CDW} down to 5 K, and our measured intensity of the higher frequency mode keeps increasing from 5 K to 80 K.

In contrast to pure CsV_3Sb_5 , the investigation of TR-reflectivity on $\text{CsV}_3\text{Sb}_{5-x}\text{Sn}_x$ with $x = 0.03-0.04$ uncovers a different CDW structural reconstruction from CsV_3Sb_5 . Fig. 7b shows the coherent phonon spectrum extracted from $\Delta R/R$ vs. time delay (Fig. 7a) in this $x = 0.03-0.04$ Sn-doped sample. Similar to CsV_3Sb_5 , at $T = 3.5$ K, the most prominent modes are at 1.34, 3.11 and 4.18 THz, along with weaker peaks around 1.80 and 3.8 THz. However, in contrast to dual modes at 1.3 THz in CsV_3Sb_5 , we observe only one mode at 1.34 THz in this Sn-doped sample, with its frequency matching the higher frequency peak in the 1.3 THz dual mode in undoped CsV_3Sb_5 (Fig. 7d). Meanwhile, the 3.11 THz mode is weaker and broader compared to CsV_3Sb_5 , making its dual mode feature weaker. We then compare our detected phonon modes with the DFT-calculated fully-symmetric phonon spectrum in various CDW phases

(Fig. 7c). Overall, the phonon spectrum of ISD + ISD with interlayer π -phase shift matches the experimental results better, since the observed 1.34, 1.80 and 3.11 THz modes are better matched in frequency. We thus conclude the actual CDW structure of this $x = 0.03$ -0.04 sample to be ISD + ISD with interlayer π -phase shift, breaking C_6 rotational symmetry as well. This matches with recent ARPES[30] and X-ray diffraction[72] results. Thus, our observed 1.34 THz mode corresponds to the calculated 1.21 THz A_g mode which is a Cs-related mode, and our observed 1.80 THz mode corresponds to the calculated 1.67 THz A_g mode which involves V and Sb oscillations (Fig. 7e). The CDW structure in this $x = 0.03$ -0.04 sample contrasts with the coexistence of SD and ISD distortion in undoped CsV_3Sb_5 , which explains the evolution from dual modes to single mode at 1.3 THz by $x = 0.03$ -0.04 Sn-doping.

In conclusion, we have studied coherent phonon excitation in CsV_3Sb_5 via time-resolved reflectivity to determine the structural configuration of its CDW phase. The phonon spectra confirm six-fold rotational symmetry breaking and the coexistence of SD and ISD distortion in the CDW phase of CsV_3Sb_5 . Meanwhile, an $x = 0.03$ -0.04 Sn-doping changes the CDW structure to ISD + ISD with interlayer π -phase shift, reducing 1.3 THz dual modes in undoped CsV_3Sb_5 to a single mode. This observation provides deeper insights for comprehending the interplay with other electronic phases in this system, such as the in-plane 1×4 unidirectional charge

order[18, 44, 73], electronic nematicity, and superconductivity. We also envision our methodology will promote the understanding of the CDW phase diagram in doped AV_3Sb_5 [72, 74, 75] and other Kagome systems such as FeGe [76, 77], and stimulate further research on ultrafast manipulation of these symmetry-breaking states.

I. ACKNOWLEDGEMENT

The construction of the pump-probe setup was supported by the Air Force Office of Scientific Research under award no. FA9550-22-1-0410. Q.D. was mainly supported by the Vagelos Institute of Energy Science and Technology graduate fellowship and also partly supported by the Air Force Office of Scientific Research under award no. FA9550-22-1-0410 and the NSF EPM program under grant no. DMR-2213891. S.D.W. and B.R.O. gratefully acknowledge support via the UC Santa Barbara NSF Quantum Foundry funded via the Q-AMASE-i program under award DMR-1906325. B.R.O. thanks support from the U.S. Department of Energy (DOE), Office of Science, Basic Energy Sciences (BES), Materials Sciences and Engineering Division. B.Y. acknowledges the financial support by the Israel Science Foundation (ISF: 2932/21, 2974/23), German Research Foundation (DFG, CRC-183, A02), and by a research grant from the Estate of Gerald Alexander.

-
- [1] Ortiz, B. R. et al. New kagome prototype materials: discovery of kv 3 sb 5, rbv 3 sb 5, and csv 3 sb 5. *Physical Review Materials* **3**, 094407 (2019).
- [2] Ortiz, B. R. et al. Cs v 3 sb 5: A z 2 topological kagome metal with a superconducting ground state. *Physical Review Letters* **125**, 247002 (2020).
- [3] Ortiz, B. R. et al. Superconductivity in the z 2 kagome metal kv 3 sb 5. *Physical Review Materials* **5**, 034801 (2021).
- [4] Yin, Q. et al. Superconductivity and normal-state properties of kagome metal rbv3sb5 single crystals. *Chinese Physics Letters* **38**, 037403 (2021).
- [5] Mielke III, C. et al. Time-reversal symmetry-breaking charge order in a kagome superconductor. *Nature* **602**, 245–250 (2022).
- [6] Jiang, Y.-X. et al. Unconventional chiral charge order in kagome superconductor kv3sb5. *Nature materials* **20**, 1353–1357 (2021).
- [7] Xing, Y. et al. Optical manipulation of the charge-density-wave state in rbv3sb5. *Nature* 1–7 (2024).
- [8] Guo, C. et al. Switchable chiral transport in charge-ordered kagome metal csv3sb5. *Nature* **611**, 461–466 (2022).
- [9] Xu, Y. et al. Three-state nematicity and magneto-optical kerr effect in the charge density waves in kagome superconductors. *Nature physics* **18**, 1470–1475 (2022).
- [10] Park, T., Ye, M. & Balents, L. Electronic instabilities of kagome metals: saddle points and landau theory. *Physical Review B* **104**, 035142 (2021).
- [11] Feng, X., Jiang, K., Wang, Z. & Hu, J. Chiral flux phase in the kagome superconductor av3sb5. *Science bulletin* **66**, 1384–1388 (2021).
- [12] Denner, M. M., Thomale, R. & Neupert, T. Analysis of charge order in the kagome metal a v 3 sb 5 (a= k, rb, cs). *Physical Review Letters* **127**, 217601 (2021).
- [13] Lin, Y.-P. & Nandkishore, R. M. Complex charge density waves at van hove singularity on hexagonal lattices: Haldane-model phase diagram and potential realization in the kagome metals a v 3 sb 5 (a= k, rb, cs). *Physical Review B* **104**, 045122 (2021).
- [14] Guo, C. et al. Correlated order at the tipping point in the kagome metal csv3sb5. *Nature Physics* 1–6 (2024).
- [15] Christensen, M. H., Birol, T., Andersen, B. M. & Fernandes, R. M. Loop currents in a v 3 sb 5 kagome metals: Multipolar and toroidal magnetic orders. *Physical Review B* **106**, 144504 (2022).
- [16] Tazai, R., Yamakawa, Y. & Kontani, H. Drastic magnetic-field-induced chiral current order and emergent current-bond-field interplay in kagome metals. *Proceedings of the National Academy of Sciences* **121**, e2303476121 (2024).
- [17] Nie, L. et al. Charge-density-wave-driven electronic nematicity in a kagome superconductor. *Nature* **604**, 59–64 (2022).
- [18] Li, H. et al. Unidirectional coherent quasiparticles in the high-temperature rotational symmetry broken phase

- of a $v3sb5$ kagome superconductors. *Nature Physics* **19**, 637–643 (2023).
- [19] Xiang, Y. et al. Twofold symmetry of c -axis resistivity in topological kagome superconductor $csv3sb5$ with in-plane rotating magnetic field. *Nature communications* **12**, 6727 (2021).
- [20] Wulferding, D. et al. Emergent nematicity and intrinsic versus extrinsic electronic scattering processes in the kagome metal $csv3sb5$. *Physical Review Research* **4**, 023215 (2022).
- [21] Asaba, T. et al. Evidence for an odd-parity nematic phase above the charge-density-wave transition in a kagome metal. *Nature Physics* 1–7 (2024).
- [22] Liu, Z. et al. Absence of $e2g$ nematic instability and dominant $a1g$ response in the kagome metal $csv3sb5$. *Physical Review X* **14**, 031015 (2024).
- [23] Chen, H. et al. Roton pair density wave in a strong-coupling kagome superconductor. *Nature* **599**, 222–228 (2021).
- [24] Liang, Z. et al. Three-dimensional charge density wave and surface-dependent vortex-core states in a kagome superconductor $csv3sb5$. *Physical Review X* **11**, 031026 (2021).
- [25] Li, H. et al. Observation of unconventional charge density wave without acoustic phonon anomaly in kagome superconductors $av3sb5$ ($a=rb, cs$). *Physical Review X* **11**, 031050 (2021).
- [26] Ortiz, B. R. et al. Fermi surface mapping and the nature of charge-density-wave order in the kagome superconductor $csv3sb5$. *Physical Review X* **11**, 041030 (2021).
- [27] Christensen, M. H., Birol, T., Andersen, B. M. & Fernandes, R. M. Theory of the charge density wave in a $v3sb5$ kagome metals. *Physical Review B* **104**, 214513 (2021).
- [28] Ritz, E. T., Fernandes, R. M. & Birol, T. Impact of sb degrees of freedom on the charge density wave phase diagram of the kagome metal $csv3sb5$. *Physical Review B* **107**, 205131 (2023).
- [29] Tan, H., Liu, Y., Wang, Z. & Yan, B. Charge density waves and electronic properties of superconducting kagome metals. *Physical review letters* **127**, 046401 (2021).
- [30] Kang, M. et al. Charge order landscape and competition with superconductivity in kagome metals. *Nature Materials* **22**, 186–193 (2022).
- [31] Subires, D. et al. Order-disorder charge density wave instability in the kagome metal (cs, rb) $v3sb5$. *Nature Communications* **14**, 1015 (2023).
- [32] Hu, Y. et al. Coexistence of trihexagonal and star-of-david pattern in the charge density wave of the kagome superconductor $av3sb5$. *Physical Review B* **106**, L241106 (2022).
- [33] Li, C. et al. Coexistence of two intertwined charge density waves in a kagome system. *Physical Review Research* **4**, 033072 (2022).
- [34] Azoury, D. et al. Direct observation of the collective modes of the charge density wave in the kagome metal $csv3sb5$. *Proceedings of the National Academy of Sciences* **120**, e2308588120 (2023).
- [35] Miao, H. et al. Geometry of the charge density wave in the kagome metal $av3sb5$. *Physical Review B* **104**, 195132 (2021).
- [36] Ratcliff, N., Hallett, L., Ortiz, B. R., Wilson, S. D. & Harter, J. W. Coherent phonon spectroscopy and interlayer modulation of charge density wave order in the kagome metal $csv3sb5$. *Physical Review Materials* **5**, L111801 (2021).
- [37] Xiao, Q. et al. Coexistence of multiple stacking charge density waves in kagome superconductor $csv3sb5$. *Physical Review Research* **5**, L012032 (2023).
- [38] Wang, Y., Wu, T., Li, Z., Jiang, K. & Hu, J. Structure of the kagome superconductor $csv3sb5$ in the charge density wave state. *Physical Review B* **107**, 184106 (2023).
- [39] Jin, F. et al. π phase interlayer shift and stacking fault in the kagome superconductor $csv3sb5$. *Physical Review Letters* **132**, 066501 (2024).
- [40] Kautzsch, L. et al. Structural evolution of the kagome superconductors $av3sb5$ ($a=k, rb, cs$) through charge density wave order. *Physical Review Materials* **7**, 024806 (2023).
- [41] Stahl, Q. et al. Temperature-driven reorganization of electronic order in $csv3sb5$. *Physical Review B* **105**, 195136 (2022).
- [42] Plumb, J. et al. Phase-separated charge order and twinning across length scales in $csv3sb5$. *Physical Review Materials* **8**, 093601 (2024).
- [43] Wu, Q. et al. Simultaneous formation of two-fold rotation symmetry with charge order in the kagome superconductor $csv3sb5$ by optical polarization rotation measurement. *Physical Review B* **106**, 205109 (2022).
- [44] Zhao, H. et al. Cascade of correlated electron states in the kagome superconductor $csv3sb5$. *Nature* **599**, 216–221 (2021).
- [45] Chen, Q., Chen, D., Schnelle, W., Felser, C. & Gaulin, B. Charge density wave order and fluctuations above t_{cdw} and below superconducting t_c in the kagome metal $csv3sb5$. *Physical Review Letters* **129**, 056401 (2022).
- [46] Zhong, Y. et al. Unveiling van hove singularity modulation and fluctuated charge order in kagome superconductor $csv3sb5$ via time-resolved arpes. *Physical Review Research* **6**, 043328 (2024).
- [47] Shen, Y.-R. Principles of nonlinear optics (1984).
- [48] Shen, Y. R. & Bloembergen, N. Theory of stimulated brillouin and raman scattering. *Physical Review* **137**, A1787 (1965).
- [49] Giordmaine, J. A. & Kaiser, W. Light scattering by coherently driven lattice vibrations. *Physical Review* **144**, 676 (1966).
- [50] Wang, Z. X. et al. Unconventional charge density wave and photoinduced lattice symmetry change in the kagome metal $csv3sb5$ probed by time-resolved spectroscopy. *Phys. Rev. B* **104**, 165110 (2021).
- [51] Uykur, E. et al. Low-energy optical properties of the nonmagnetic kagome metal $csv3sb5$. *Physical Review B* **104**, 045130 (2021).
- [52] Joshi, J. et al. Short-range charge density wave order in $2h-tas2$. *Physical Review B* **99**, 245144 (2019).
- [53] Liu, G. et al. Observation of anomalous amplitude modes in the kagome metal $csv3sb5$. *Nature communications* **13**, 3461 (2022).
- [54] He, G. et al. Anharmonic strong-coupling effects at the origin of the charge density wave in $csv3sb5$. *Nature Communications* **15**, 1895 (2024).
- [55] Stojchevska, L., Mertelj, T., Chu, J.-H., Fisher, I. R. & Mihailovic, D. Doping dependence of femtosecond quasiparticle relaxation dynamics in $ba(fe, co)2as2$ single crystals: Evidence for normal-state nematic fluctuations.

- Physical Review B **86**, 024519 (2012).
- [56] Thewalt, E. *et al.* Imaging anomalous nematic order and strain in optimally doped bafe 2 (as, p) 2. *Physical review letters* **121**, 027001 (2018).
- [57] Liu, S. *et al.* Transient electronic anisotropy in overdoped naf e 1- x c ox as superconductors. *Physical Review B* **97**, 020505 (2018).
- [58] Merlin, R. Generating coherent thz phonons with light pulses. *Solid state communications* **102**, 207–220 (1997).
- [59] Stevens, T., Kuhl, J. & Merlin, R. Coherent phonon generation and the two stimulated raman tensors. *Physical Review B* **65**, 144304 (2002).
- [60] Dhar, L., Rogers, J. A. & Nelson, K. A. Time-resolved vibrational spectroscopy in the impulsive limit. *Chemical Reviews* **94**, 157–193 (1994).
- [61] Yan, Y.-X., Gamble Jr, E. B. & Nelson, K. A. Impulsive stimulated scattering: General importance in femtosecond laser pulse interactions with matter, and spectroscopic applications. *The Journal of chemical physics* **83**, 5391–5399 (1985).
- [62] Gray, I. *et al.* Time-resolved magneto-optical effects in the altermagnet candidate mnTe. *Applied Physics Letters* **125** (2024).
- [63] Cheng, T. *et al.* Mechanism for displacive excitation of coherent phonons in sb, bi, te, and ti2o3. *Applied Physics Letters* **59**, 1923–1925 (1991).
- [64] Zeiger, H. *et al.* Theory for displacive excitation of coherent phonons. *Physical Review B* **45**, 768 (1992).
- [65] De Silvestri, S. *et al.* Femtosecond time-resolved measurements of optic phonon dephasing by impulsive stimulated raman scattering in α -perylene crystal from 20 to 300 k. *Chemical physics letters* **116**, 146–152 (1985).
- [66] Ruhman, S., Joly, A. G. & Nelson, K. A. Time-resolved observations of coherent molecular vibrational motion and the general occurrence of impulsive stimulated scattering. *The Journal of chemical physics* **86**, 6563–6565 (1987).
- [67] Wu, S. *et al.* Charge density wave order in the kagome metal av_3sb_5 (a= cs, rb, k). *Physical Review B* **105**, 155106 (2022).
- [68] Nakayama, K. *et al.* Multiple energy scales and anisotropic energy gap in the charge-density-wave phase of the kagome superconductor csv_3sb_5 . *Physical Review B* **104**, L161112 (2021).
- [69] Zhou, X. *et al.* Origin of charge density wave in the kagome metal csv_3sb_5 as revealed by optical spectroscopy. *Physical Review B* **104**, L041101 (2021).
- [70] Wang, Z. *et al.* Distinctive momentum dependent charge-density-wave gap observed in csv_3sb_5 superconductor with topological kagome lattice. *arXiv preprint arXiv:2104.05556* (2021).
- [71] Ning, H. *et al.* Dynamical decoding of the competition between charge density waves in a kagome superconductor. *Nature Communications* **15**, 7286 (2024).
- [72] Kautzsch, L. *et al.* Incommensurate charge-stripe correlations in the kagome superconductor csv_3sb_5 -x sn x. *npj Quantum Materials* **8**, 37 (2023).
- [73] Wang, Z. *et al.* Electronic nature of chiral charge order in the kagome superconductor cs_v_3sb_5 . *Physical Review B* **104**, 075148 (2021).
- [74] Oey, Y. M. *et al.* Fermi level tuning and double-dome superconductivity in the kagome metal csv_3sb_5 -x sn x. *Physical Review Materials* **6**, L041801 (2022).
- [75] Zhong, Y. *et al.* Nodeless electron pairing in csv_3sb_5 -derived kagome superconductors. *Nature* **617**, 488–492 (2023).
- [76] Teng, X. *et al.* Discovery of charge density wave in a kagome lattice antiferromagnet. *Nature* **609**, 490–495 (2022).
- [77] Oh, J. S. *et al.* Tunability of charge density wave in a magnetic kagome metal. *arXiv preprint arXiv:2404.02231* (2024).